ORNL/TM-7258

ornl

OAK
RIDGE
NATIONAL
LABORATORY

UNION
CARBIDE

High-Power Laser and Arc Welding of Thorium-Doped Iridium Alloys

S. A. David
C. T. Liu

OPERATED BY
UNION CARBIDE CORPORATION
FOR THE UNITED STATES
DEPARTMENT OF ENERGY

DISCLAIMER

Printed in the United States of America. Available from
National Technical Information Service
U.S. Department of Commerce
5285 Port Royal Road, Springfield, Virginia 22161
NTIS price codes—Printed Copy: A03 Microfiche A01

ORNL/TM-7258

Contract No. W-7405-eng-26

METALS AND CERAMICS DIVISION

HIGH-POWER LASER AND ARC WELDING OF THORIUM-DOPED IRIDIUM ALLOYS

S. A. David and C. T. Liu

Date Published: May 1980

NOTICE This document contains information of a preliminary nature. It is subject to revision or correction and therefore does not represent a final report.

OAK RIDGE NATIONAL LABORATORY
Oak Ridge, Tennessee 37830
operated by
UNION CARBIDE CORPORATION
for the
DEPARTMENT OF ENERGY

page blank

CONTENTS

HIGH-POWER LASER AND ARC WELDING OF THORIUM-DOPED IRIDIUM ALLOYS

S. A. David and C. T. Liu

ABSTRACT

The arc and laser weldabilities of two Ir—0.3% W alloys containing 60 and 200 wt ppm Th have been investigated. The Ir—0.3% W alloy containing 200 wt ppm Th is severely prone to hot cracking during gas tungsten-arc welding. Weld metal cracking results from the combined effects of heat-affected zone liquation cracking and solidification cracking. Scanning electron microscopic analysis of the fractured surface revealed patches of low-melting eutectic. The cracking is influenced to a great extent by the fusion zone microstructure and thorium content. This alloy has been welded with a continuous-wave high-power CO_2 laser system with beam power ranging from 5 to 10 kW and welding speeds of 8 to 25 mm/s. Successful laser welds without hot cracking have been obtained in this particular alloy. This is attributable to the highly concentrated heat source available in the laser beam and the refinement in fusion zone microstructure obtained during laser welding.

Efforts to refine the fusion zone structure during gas tungsten-arc welding of Ir—0.3 % W alloy containing 60 wt ppm Th were partially successful. Here transverse arc oscillation during gas tungsten-arc welding refines the fusion zone structure to a certain extent. However, microstructural analysis of this alloy's laser welds indicates further refinement in the fusion zone microstructure than in that from the gas tungsten-arc process using arc oscillations. The fusion zone structure of the laser weld is a strong function of welding speed.

INTRODUCTION

The Ir—0.3 % W alloys doped with about 50 wt ppm Th are currently used as postimpact containment material for radioactive fuel in thermoelectric generators that provide stable electrical power for a variety of outer planetary missions.[1] Iridium alloys were chosen for this application because of their high melting point, good high-temperature strength, oxidation resistance, and compatibility with oxide fuel forms and insulation materials. Thorium has been added as a grain boundary strengthener, segregating strongly to the grain boundaries and inhibiting

intergranular fracture during severe reentry impact from space. Two promising iridum alloys containing 200 wt ppm Th (DOP-14) and 60 wt ppm Th and 50 wt ppm Al (DOP-26), respectively, have been currently developed at ORNL. The impact properties of these alloys are a strong function of grain size. Of the two alloys, DOP-14 shows better impact properties after long-term aging at fuel-clad temperatures of 1300 to 1400°C. This is related to the higher level of thorium added in DOP-14, which effectively retards the grain growth through the precipitation of $ThIr_5$ particles. However, this alloy has very poor weldability characteristics.

In the past, preliminary weldability screening studies have shown that potential iridium alloys containing at least 100 wt ppm Th, particularly DOP-14, are subject to severe hot cracking during gas tungsten-arc (GTA) welding. However, the alloys can be welded successfully by the electron beam welding (EBW) process over a narrow range of focuses.[2] In spite of its success, the vacuum requirements of the EBW process in an isolation cell during fuel encapsulation render the process impractical. Here laser welding offers a suitable alternate process to weld these alloys since the high-power laser beam can be transmitted for appreciable distance through air at standard pressures without serious power attenuation or degradation of optical quality. Also, the laser system produces a concentrated energy source that can be precisely controlled during welding.

The iridium alloys containing less than 100 wt ppm Th, particularly DOP-26, can be successfully welded by the GTA process. Nevertheless, since the impact properties of the iridium alloys in general are a strong function of grain size, the coarse unfavorable structure in GTA welds can severely reduce the ductility and impact strength of a welded joint.[3] This limits the application of these alloys. Attempts to overcome this problem have involved the judicious selection of weld process parameters to control heat input levels and solidification rate and thereby solidification structure. For iridium alloys, efforts to refine the fusion zone structure by oscillating the welding arc under controlled conditions have been somewhat successful.[4,5] The inability to control the heat source in conventional arc welding restricts the ability to achieve a weld having acceptable structures and properties. By using a continuous-wave CO_2 laser beam with continuous multikilowatt output power, it is possible

to produce a fusion weld with lower total energy input than through conventional arc welding.

Hot cracking during welding has been studied experimentally.[6–9] Different manifestations of hot cracking during welding are: (1) solidification cracking, (2) liquation cracking in the heat-affected zone (HAZ), (3) a combination of the above two, and (4) elevated-temperature (subsolidus) cracking during heat treatment of welds. A number of theories have attempted to explain the mechanism of hot cracking.[10–14] Solidification cracking in weld metal often occurs during later stages of solidification when the strains resulting from thermal and solidification contraction exceed the ductility of the partially solidified metal. Liquid pools trapped between the grains or interdendritic regions greatly influence the tensile properties of the partially solidified alloy. Also, the mechanical behavior of the partially solidified alloy determines its solidification cracking sensitivity. Solidification cracking has been known to be favored by the factors that decrease the solid-solid contact area during the last stages of solidification. Two of the most important are low-melting segregates and grain size. Low-melting segregates at the grain boundaries may exist as a liquid film to temperatures well below the equilibrium solidus and reduce the grain boundary contact area to a minimum.[15] Also, the coarser the grain structure the less the grain boundary contact areas for a given amount of nonequilibrium liquid. Hence, coarse-grained fusion zone structures are generally more prone to solidification cracking than fine-grained ones. Liquation cracking in the HAZ occurs: (1) as low-melting segregates are liquated at the grain boundaries of the base metal and (2) as tensile stresses develop in the HAZ as the welding arc passes on. Weld metal cracking may also originate from the HAZ liquation crack. Shrinkage stress, coarse fusion zone grain structure, and the presence of low-melting segregates within the weld metal could lead to weld metal cracking as an extension of the HAZ liquation crack. During our investigation cracking during heat treatment was never observed.

We describe both the feasibility of obtaining a sound weld with refined fusion zone structure in iridium alloys by using both arc welding and high-power continuous-wave CO_2 laser welding and the successful application of laser welding to eliminate hot cracking problems encountered during arc welding of iridium alloys containing more than 100 wt ppm Th.

LASERS

The "light amplification by stimulated emission of radiation" (LASER) device emits a highly collimated, coherent monochromatic beam of electromagnetic radiation in the visible region of the electromagnetic spectrum. In theory, lasing action was predicted by Townes and Schawlow[16] in 1958 and was demonstrated for the first time by Maiman in 1960 using a ruby crystal.[17] A laser beam suitably focused onto a work piece can heat, melt, or vaporize the material. Laser generating medium can be gas, liquid, or solid. Since the first successful operation of a laser, it has been advocated as a highly versatile tool for a broad range of materials processing applications, particularly fusion welding. High-power pulsed lasers have been employed in the past several years to obtain spot welds in small components. Continuous welding may be approximated with the pulsed laser by using overlapping spot welds. Laser systems have developed very rapidly in the past 15 years.[18,19] Addition of neodymium to yttrium aluminum garnet (YAG) and to yttrium aluminate (YALO) provided the solid-state lasers with a continuous-wave output capability.[20] Also, the first CO_2 laser was constructed and operated[21] in 1964. It exhibited an initial power output of several watts and was improved later by the addition of nitrogen and helium. Lasing action was improved further by the introduction of a closed-cycle convectively cooled unit[22,23] that provided sufficient continuous power output to handle significant welding tasks.[24–26] Three types of continuous-wave lasers radiating in the far infrared at a wavelength of 10.6 μm are available for materials processing operations: discharge tube, axial flow, and transverse flow (Fig. 1).

Discharge-tube lasers exhibit output power in the range 0.05 kW per meter length of lasing cavity. Laser gas is cooled by conduction to the cold-side walls of the lasing tube. Axial-flow lasers utilize a close-cycle configuration in which gas flows rapidly through the lasing chamber. Heat is removed by convection and a series of heat exchangers. Low mass flow restricts power output to about 0.7 kW per meter of lasing tube. In both discharge-tube and axial-flow lasers, discharge takes place coaxial to the flow direction. Since CO_2 lasers cannot be operated efficiently

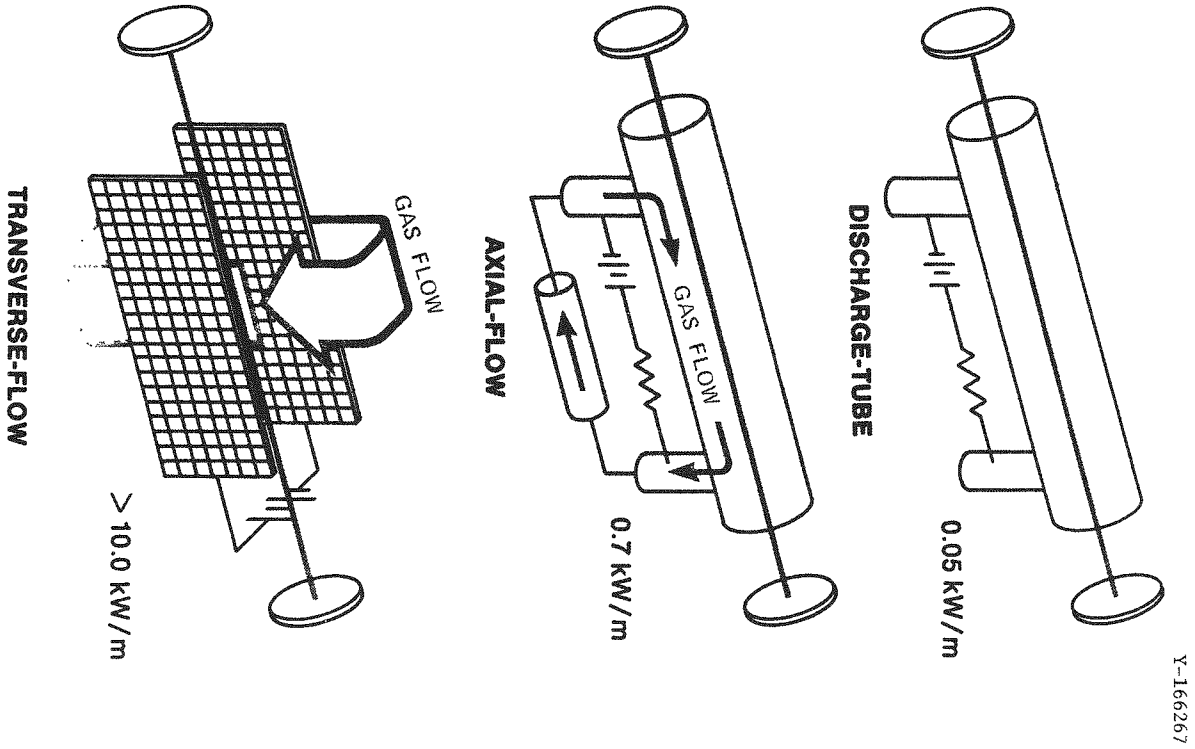

Fig. 1. Types of Electric Gas Lasers Showing Practical Limits of Laser Output Power Per Meter Length of Lasing Cavity. (Schematic courtesy of Avco Everett Research Laboratory, Inc.)

over about 200°C, both devices are limited in output power. Transverse-flow lasers feature mutually perpendicular gas flow, electrical discharge, and optical axes. This design shortens the dwell time of the lasing gas in the optical cavity by providing the conditions necessary for higher power density and thus more power per unit length of laser chamber.

EXPERIMENTAL PROCEDURE

Autogenous bead-on-plate and butt welds were made by using 0.65-mm-thick DOP-14 and DOP-26 coupons with other dimensions variable to investigate the laser weldability of these alloys with an Avco HPL* multikilowatt CO_2 laser. This laser is a transverse-flow device that has a nominal rating of 15-kW continuous output power. A schematic of the laser is

*Registered trademark of Avco Everett Research Laboratory, Inc., 2385 Revere Beach Parkway, Everett, MA 02149.

is shown in Fig. 2. Welds* were made with laser output power ranging from 5 to 10 kW and with welding speeds 8.0 to 25.0 mm/s by using a 66-mm (2.6-in.) annular beam output mode. This was focused through an F/18 telescope. The welding fixture used for welding is shown in Fig. 3. During welding shielding was provided by helium gas flowing through an off-axis diffuser at 5.6 m^3/h. Table 1 shows various parameters used during laser welding.

Gas tungsten-arc welds with and without arc oscillations were made inside a large controlled-atmosphere dry box containing the necessary welding fixtures (Fig. 4). Welds were made in 75% He—25% Ar by using a stationary arc over a travel carriage with variable speed control. Arc oscillations were obtained by using a commercially available oscillator with a magnetic probe. Arc oscillations both in the direction of welding (longitudinal) and normal to the welding direction (transverse) were evaluated by using constant amplitude and dwell time. Based on an initial experiment involving a range of frequencies[5] and earlier study,[4] a transverse oscillation frequency of 375 cycles/min was selected and used in this investigation. The arc welding parameters used are listed below:

Electrode	1.6 mm (1/16 in.) in diameter, 2% ThO_2—W
Electrode tip	25° included angle with 0.25 mm (0.01 in.) flat
Torch gas	He—25% Ar
Oscillations	375 cycles/min
Arc voltage	12—14 V
Current	100—115 A

*The term weld in the text refers only to autogenous bead-on-plate welds (melt runs), unless stated otherwise.

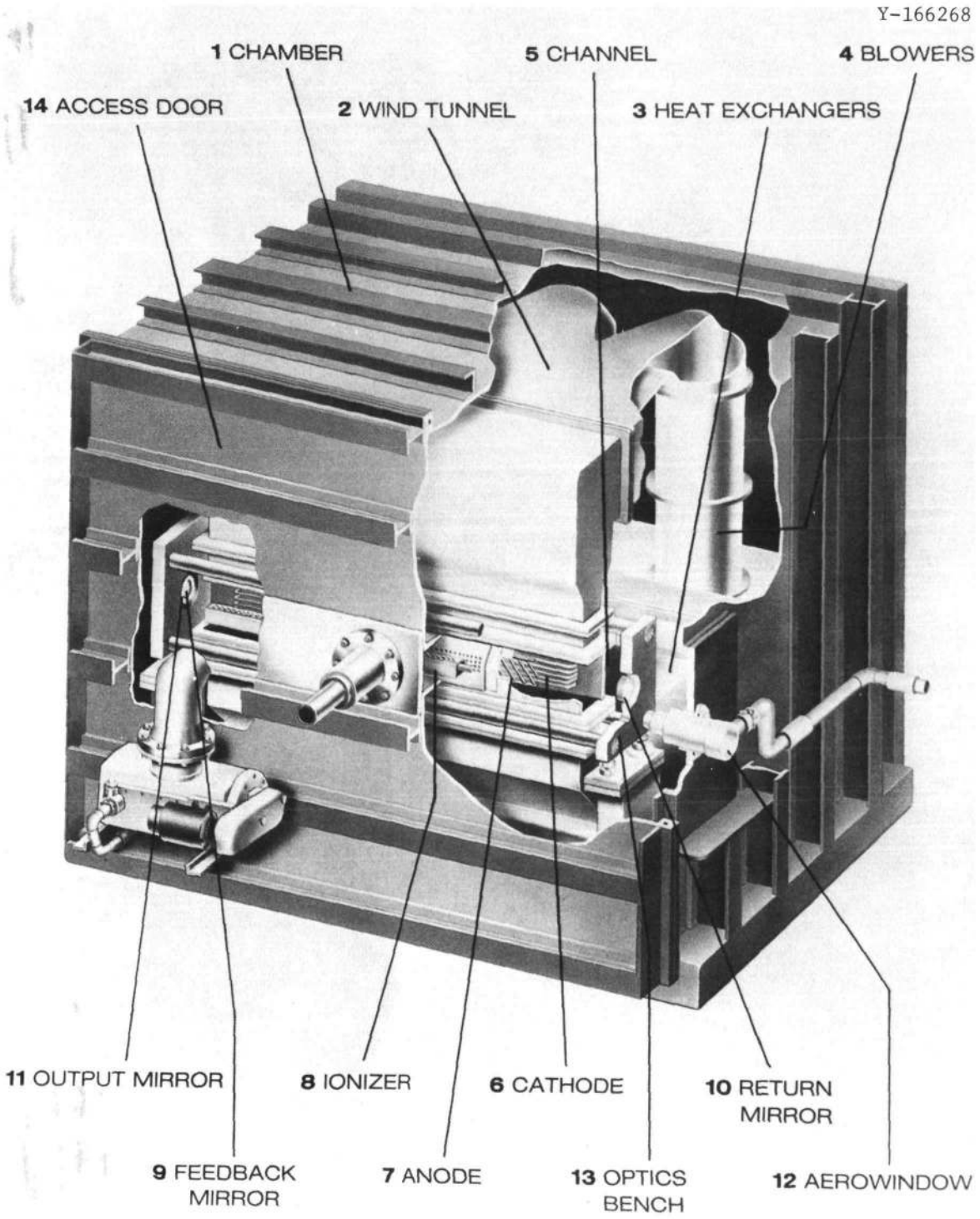

Fig. 2. Schematic of an Avco HPL Laser. Schematic courtesy of Avco Everett Medslworking Lasers, Inc.

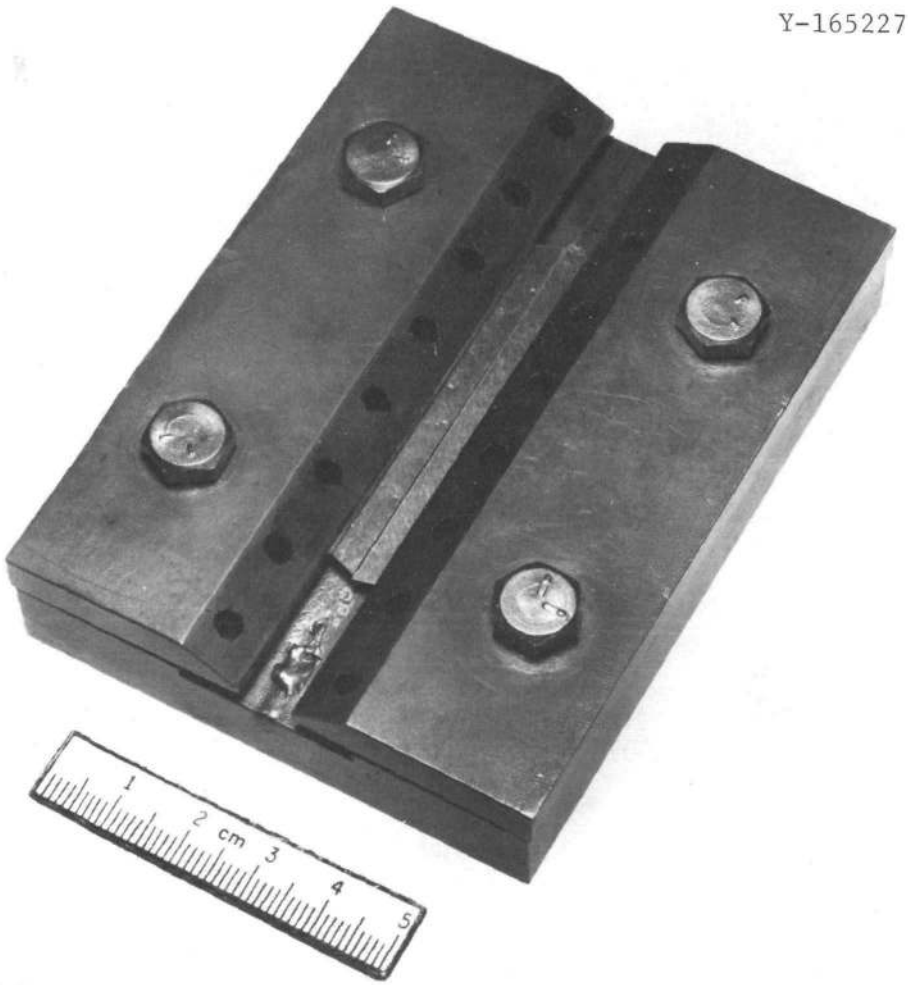

Fig. 3. Welding Fixture Used to Make Autogenous Bead-On-Plate and Butt Welds.

Table 1. Laser Welding Parameters[a]

Specimen	Power on Work (kW)	Welding Speed (mm/s)	Bead Width, mm (Top)	Bead Width, mm (Root)	Type of Weld
		Alloy DOP-26			
1A	4.8	8.3	1.97	1.5	Melt run
2A	6.0	12.5	2.2	1.6	Melt run
3A	7.0	16.7	2.0	1.5	Melt run
4A	5.2	8.3	2.4	1.7	Butt weld
5A	6.0	12.5	2.2	1.8	Butt weld
6A	7.1	16.7	2.1	1.7	Butt weld
		Alloy DOP-14			
21A	5.0	8.3	2.4	1.9	Melt run
22A	5.8	12.5			Melt run
23A	6.0	12.5			Melt run
24A	8.6	25.0			Melt run
25A	5.8	12.5	2.2	1.6	Butt weld
26A	8.7	25.0	1.8	1.1	Butt weld

[a]Focus for all welds was 980 mm.

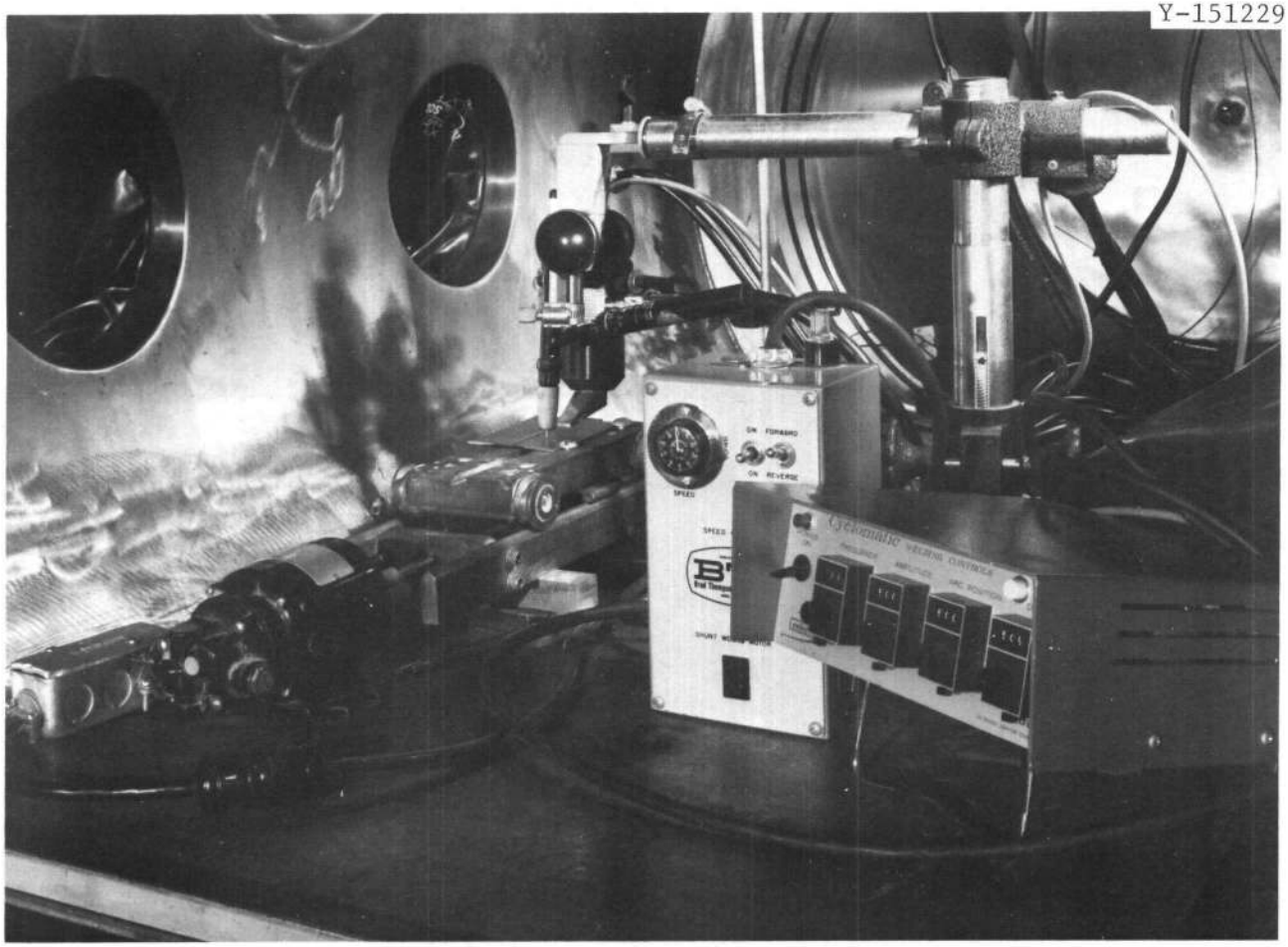

Fig. 4. Welding Setup Inside a Dry Box Showing Tungsten Electrode, Magnetic Probe, Travel Carriage, and the Arc Oscillator Control.

Various sections of the welds were prepared for metallographic observations by standard techniques. The samples were etched electrolytically in a solution of 400 ml H_2O, 100 ml HCL, and 50 g NaCl in a stainless steel container with an ac power supply.

DOP-14 WELD METAL MICROSTRUCTURE

Arc Welds

Earlier studies have shown that the Ir—0.3 % W alloy containing 200 wt ppm Th is prone to severe hot cracking during both arc welding and EBW with a highly defocused beam.[2]

As discussed earlier, the hot-cracking susceptibility of an alloy depends on elemental composition, distribution of elements, and the microstructural characteristics within the material. During arc welding of the iridium alloy DOP-14 the resulting fusion zone grain structure and segregation characteristics were very critical in determining the hot-cracking susceptibility of the alloy. In an earlier study[2] on EBW of an iridium alloy similar in composition to DOP-14 with a highly defocused beam, the weld metal cracked severely. The crack predominantly followed the centerline of the weld metal. Also, the crack path was mostly intergranular. A close examination of the microstructures and crack path indicated that the microcrack had initiated in the HAZ* as a liquation crack. Aided by conditions such as coarse fusion zone grain structure and low-melting segregates within the fusion zone, the HAZ liquation crack had promoted weld metal cracking. Similar observations have been made during GTA welding of DOP-14 alloy. Figure 5 shows macrostructure and transverse microstructure of an autogenous bead-on-plate weld made without arc oscillation. The microstructure was observed to be very coarse and is typical of arc welds made on this high-temperature alloy. In particular, along the centerline of the weld one or two grains often span the thickness of the

*For this high-temperature alloy the HAZ is very narrow and ill defined.

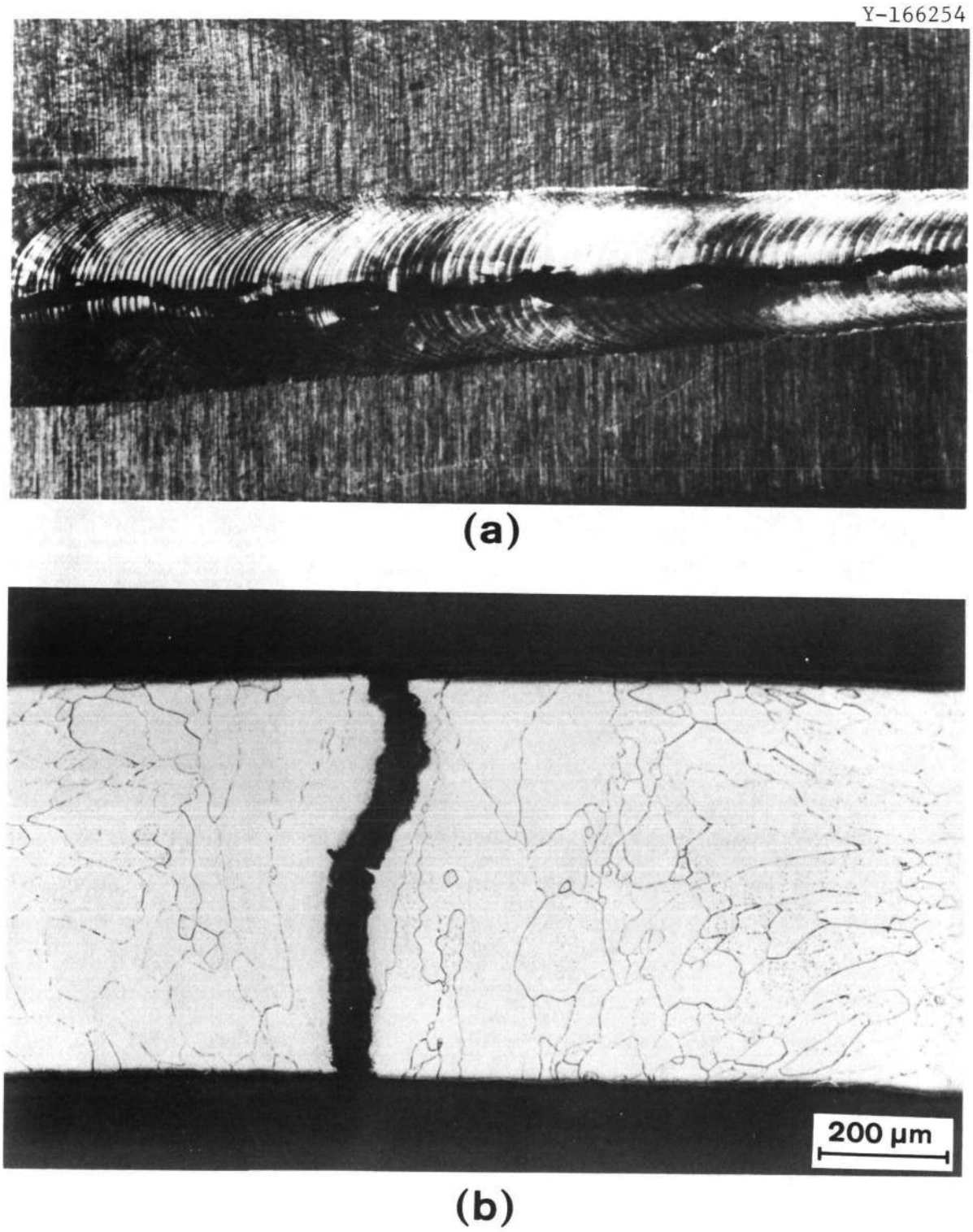

Fig. 5. Autogenous Bead-on-Plate Weld. Welding speed: 2.5 mm/s. (a) Macrostructure. (b) Transverse microstructure of the weld.

sample. Also, the grains are oriented such that the grain boundary is normal to the thermal and solidification shrinkage stress axis. The cracking predominantly follows the centerline of the weld and is mostly intergranular. A close observation of the microstructure and crack path indicated that the crack had initiated in the HAZ as a liquation crack. This possibly results from melting in the highly thorium-segregated base metal grain boundaries to a distance determined by both the thermal gradient normal to the weld and the tensile stresses that develop in the HAZ as the welding arc passes on. As mentioned earlier, thorium in this alloy has been added as a grain boundary strengthener. Also, preferential segregation of thorium to the grain boundaries has been observed.[27] If the thorium concentration along the grain boundaries of the base metal or in the last liquid to freeze within the weld metal is high enough, it could lead to the possible formation of low-melting constituents (in the iridium-thorium system, a eutectic). Once the crack is initiated in the HAZ, it could grow normal to the fusion line and may or may not extend into the weld metal. However, in all welds examined the presence of a HAZ crack together with conditions such as a coarse fusion zone grain structure and low-melting segregates within the fusion zone seem to have led to the weld metal cracking. Figure 6 shows microscopic details of the crack initiation and subsequent growth pattern in an arc-welded DOP-14 alloy sheet. Scanning electron microscopic (SEM) examination of the cracked weld metal surface revealed a number of eutectic patches, as shown in Fig. 7. Similar observations have been made on electron beam welds that cracked during welding.[2] The observed eutectic patches relate well to the phase diagram of the iridium-thorium system,[28,29] which indicates a eutectic between iridium and Ir_5Th at about 2000°C. Here it should be pointed out that the weld metal cracking may also occur without being aided by HAZ liquation crack as a result of the rejection of low-melting solutes, namely thorium, into the liquid, which would prolong the liquid film stage during solidification of the weld metal. At this point, as mentioned

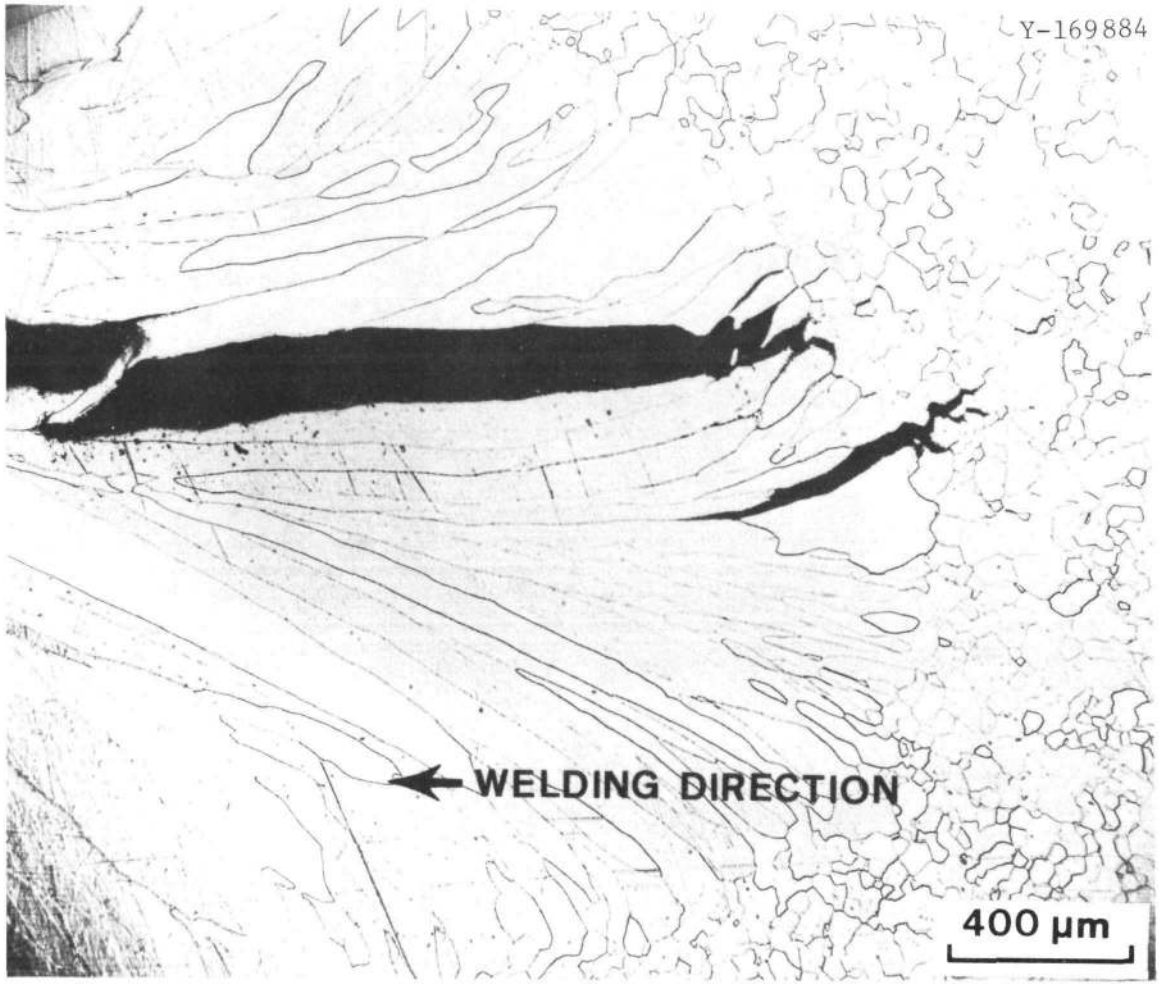

Fig. 6. Crack Nucleation in the Heat-Affected Zone at the Start of the Weld and Further Propagation into the Weld Metal in a Gas Tungsten-Arc Weld.

earlier, a very coarse fusion zone structure would add to the hot-cracking sensitivity of the alloy. However, in a majority of the welds examined during this investigation, weld metal cracking has been brought about by the nucleation and propagation of a HAZ liquation crack.

Efforts to overcome the hot-cracking problem through refinement of the fusion zone microstructure through arc oscillation and pulsed arc welding processes were not fruitful.

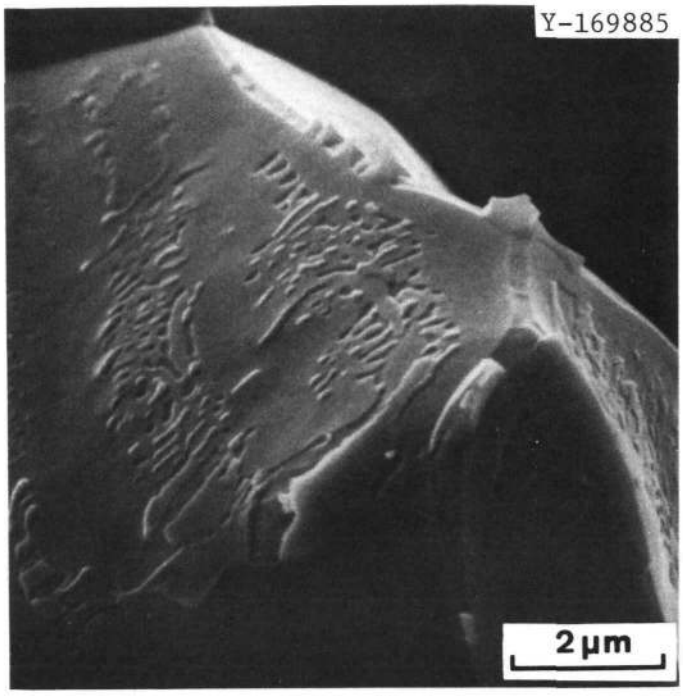

(a)

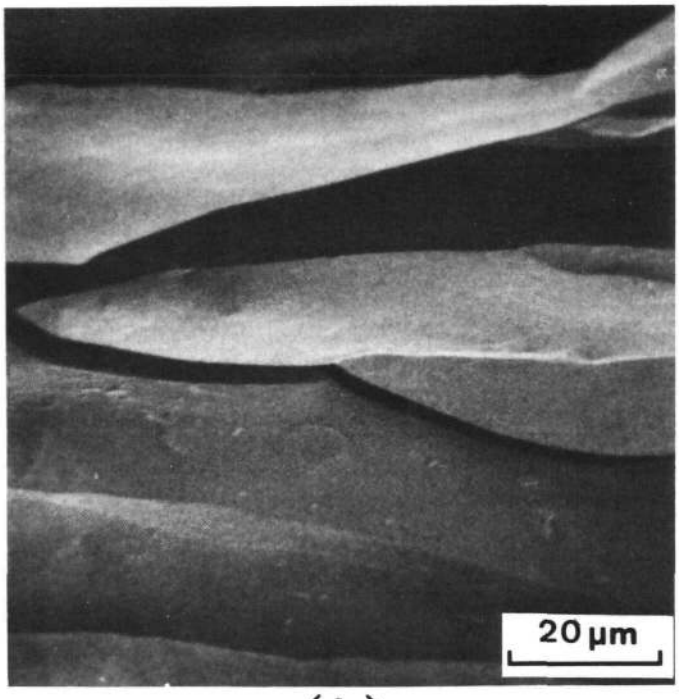

(b)

Fig. 7. Scanning Electron Micrographs Showing (a) Eutectic Patches on the Surface of the Fractured Arc Weld and (b) Absence of Eutectic Patches on the Surface of the Fractured Laser Weld by High-Velocity Impact Testing.

Laser Welds

The results of the arc and EBW studies of iridium alloys doped with over 100 wt ppm Th indicate that the heat source and fusion zone grain structure are two major factors that could influence the cracking behavior of these alloys during welding. The alloys crack severely during GTA welding or welding with a highly defocused electron beam. Here use of a laser, with its highly concentrated heat source capability, could prove to be an attractive alternate heat source to weld these alloys, particularly DOP-14.

Welds without hot cracking have been successfully made with the continuous-wave multikilowatt CO_2 laser system. Considering the two-dimensional shapes of the weld puddle as seen on the weld surface, the weld puddle could assume a teardrop shape at high welding speeds or an elliptical puddle shape at low welding speeds, as shown in Fig. 8. Typical microstructures of the DOP-14 laser welds made at 12.5 mm/s are

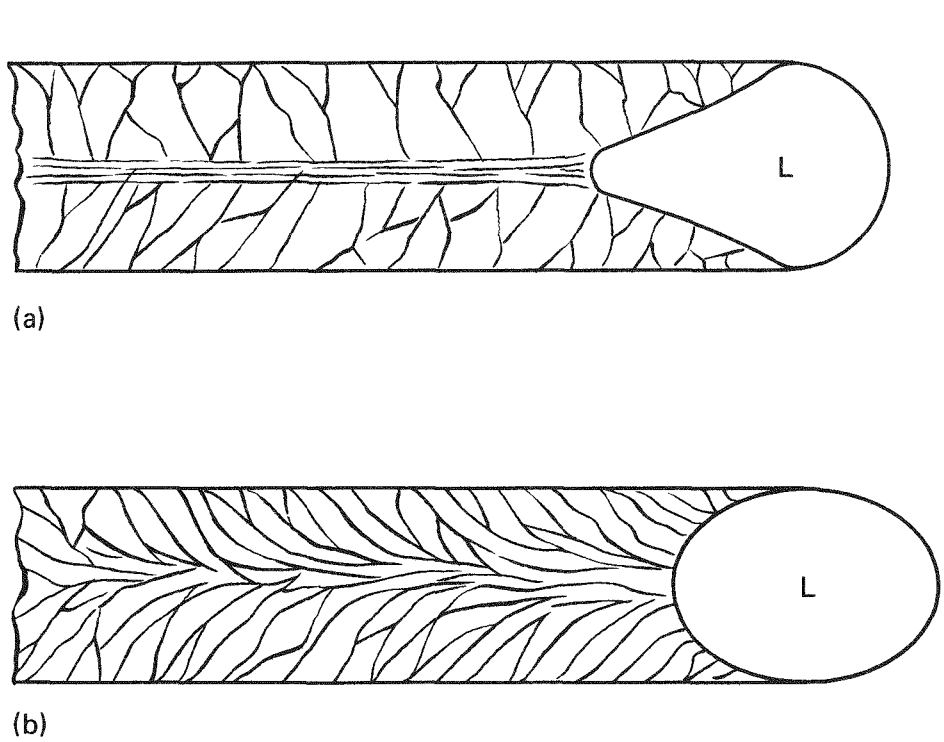

Fig. 8. Fusion Zone Grain Structure Development in (a) Teardrop-Shaped Weld Puddle and (b) Elliptical Weld Puddle.

shown in Fig. 9. At this welding speed the puddle shape appears to be elliptical. The grains in the fusion zone appear to have nucleated epitiaxially on the partially melted base metal grains and have continued to grow normal to the solid-liquid interface defined by the weld puddle shape. In the process some of the unfavorably oriented grains appear to have been eliminated. The most favorably oriented grains on either side of the fusion line continue to grow until they interact with a few grains growing along the welding direction. Transverse fusion zone microstructure [Fig. 9(b)] shows very fine grain structure within the weld. Figure 10 shows a typical microstructure of the laser weld made at 25 mm/s. The puddle shape at this welding speed appears to have assumed a teardrop. Again, the grains appear to have nucleated epitiaxially on the partially melted base metal grains and continued to grow almost normal to the centerline of the weld. Microstructure of the transverse section of the weld revealed a narrow band of fine grain structure along the centerline of the weld. This is a result of a narrow band of fine columnar grains growing at the trailing edge of the weld puddle and along the welding direction. This is shown schematically in Fig. 8(a). Welds with microstructural characteristics such as this never exhibited any hot cracking.

The successful application of the laser beam to weld DOP-14 results from the highly concentrated heat source provided by the laser beam. This highly concentrated heat source and the high thermal gradient provide solidification rates an order of magnitude faster than those associated with other conventional fusion welding techniques, leading to a finer fusion zone grain structure. Also, a highly concentrated laser beam tends to confine most of the heating to within the fusion zone, thus not contributing to the fusion of the segregates at the base metal grain boundaries. Thus a combination of reduced time for the fusion of segregates at the grain boundaries and a fine fusion zone grain structure seems to improve the weldability of DOP-14 alloy.

Successful butt welds were also made without any cracking. The fusion zone microstructures of the butt welds were observed to be similar to the autogenous laser bead-on-plate welds.

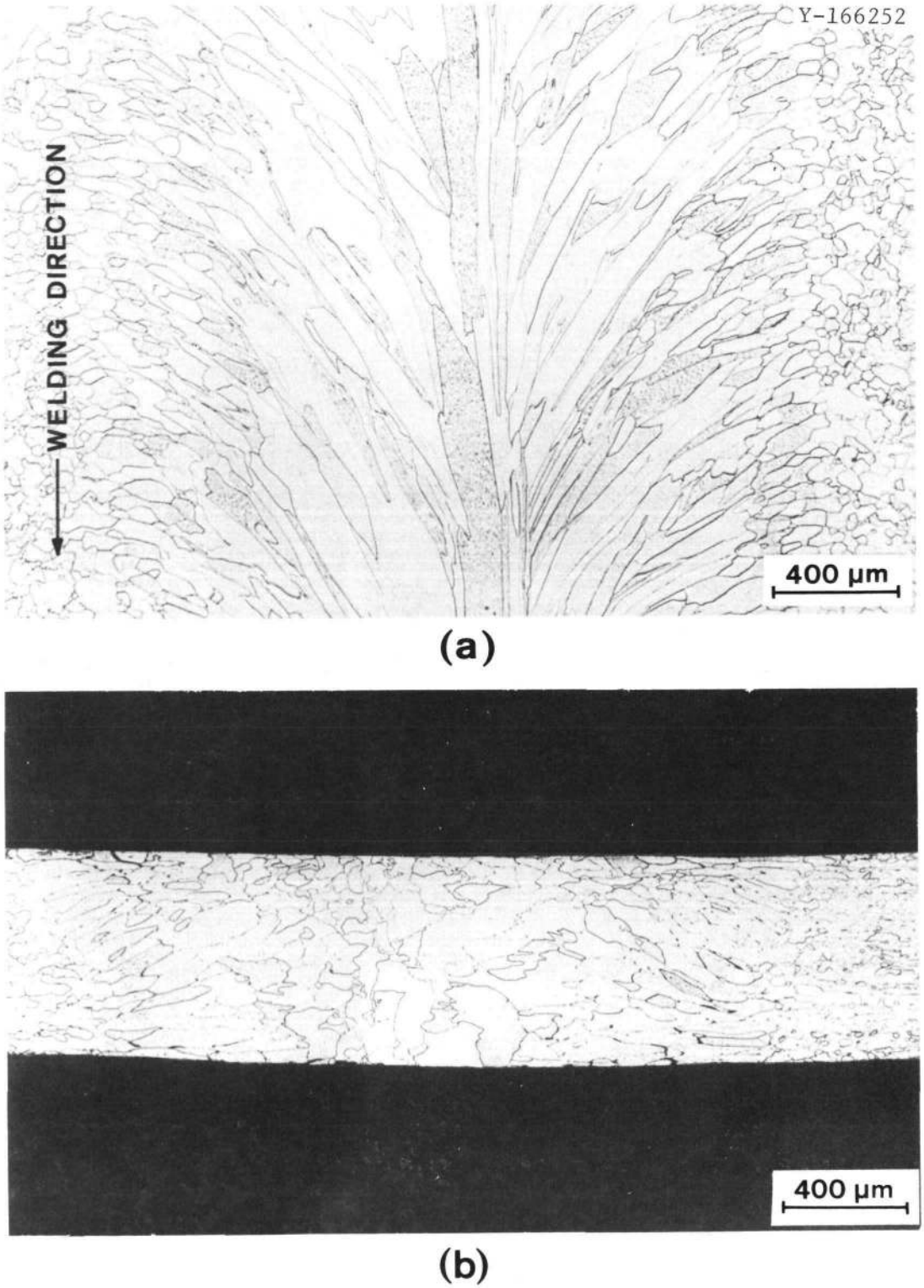

Fig. 9. Fusion Zone Microstructure of a Laser Weld. Welding speed: 12.5 mm/s. (a) Top surface. (b) Transverse section.

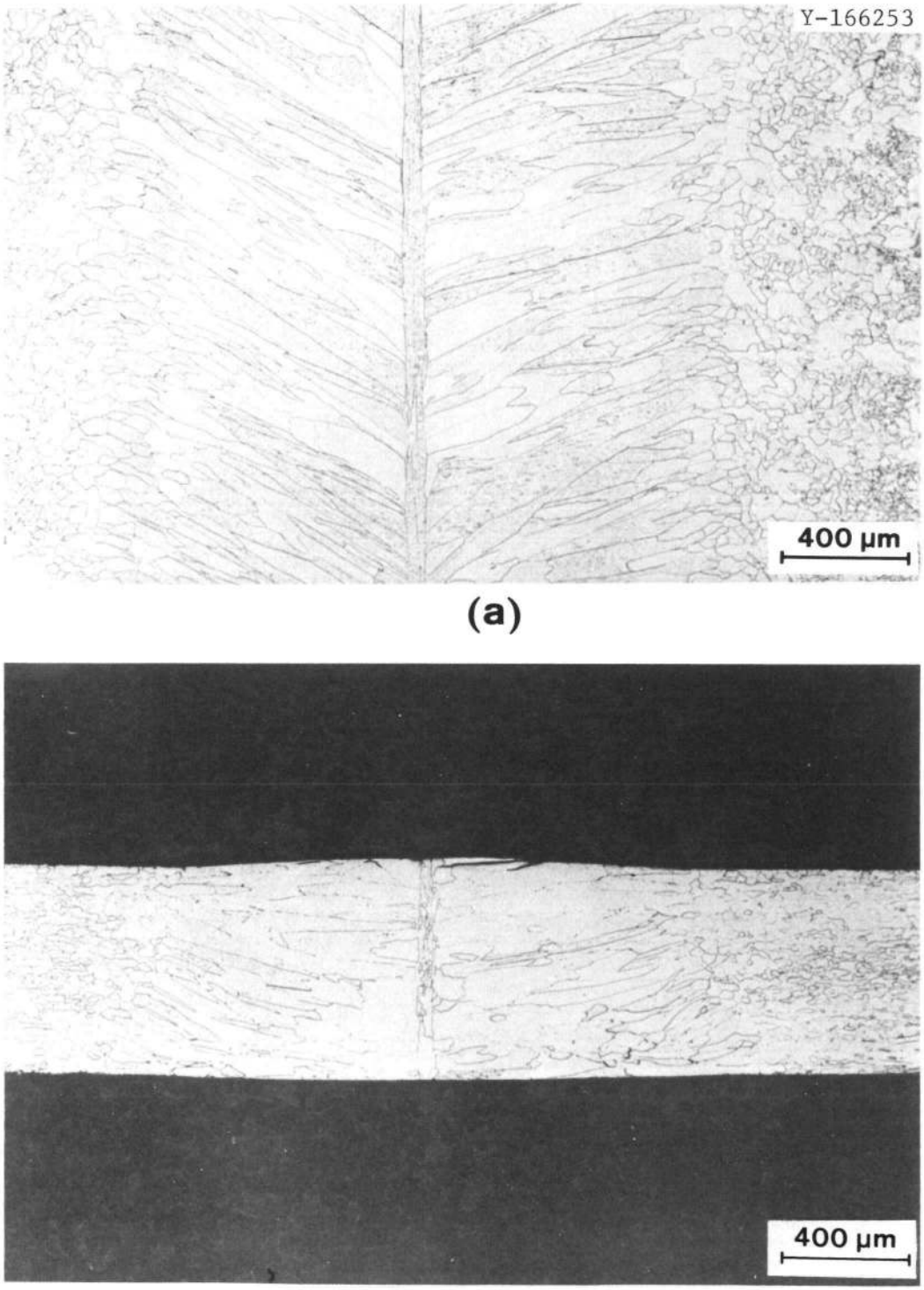

Fig. 10. Fusion Zone Microstructure of a Laser Weld. Welding speed: 25 mm/s. (a) Top surface. (b) Transverse section.

DOP-26 WELD METAL MICROSTRUCTURE

As stated earlier the existence of coarse unfavorable fusion zone solidification structure of DOP-26 GTA welds can severely reduce the ductility and impact strength of the welded joint. Hence attempts to overcome this problem included investigating various welding processes and judiciously selecting weld process parameters to control heat input levels and solidification rate and thereby solidification structure.

Arc Welds

To evaluate the effect of arc oscillation during welding, the fusion zone microstructures of the welds with and without arc oscillations were compared. Figure 11 shows surface and transverse weld microstructures of an arc weld made without arc oscillation at a welding speed of 12.5 mm/s. The overall fusion zone structure appears rather coarse except along the centerline of the weld. This is attributable to the weld puddle shape at high welding speeds and to associated weld pool solidification conditions. Structure of the fusion zone is influenced markedly by the variations in welding parameter and by associated change in weld puddle shape. The fusion zone structure shown in Fig. 11 is typical of welds made on this sheet material at high welding speeds. As discussed earlier the weld puddle could assume a teardrop shape at high welding speeds or an elliptical puddle shape at low welding speeds, as shown in Fig. 8. Generally during welding, initial growth of partially melted grains in the base metal is followed by a competitive growth process resulting from the tendency for growth to proceed most readily in grains oriented along easy growth direction with the largest component of the temperature gradient. A teardrop-shaped weld puddle has an almost invariant direction of maximum thermal gradient at all points on the pool edge from the fusion boundary to almost the weld center. This results in growth of a few favorably oriented grains at the fusion boundary at the expense of unfavorably oriented grains. Thus, only a few grains survive to grow toward the center until their growth is interrupted by grains growing along the welding direction as a result of the weld pool profile. Thus, the fine

(a)

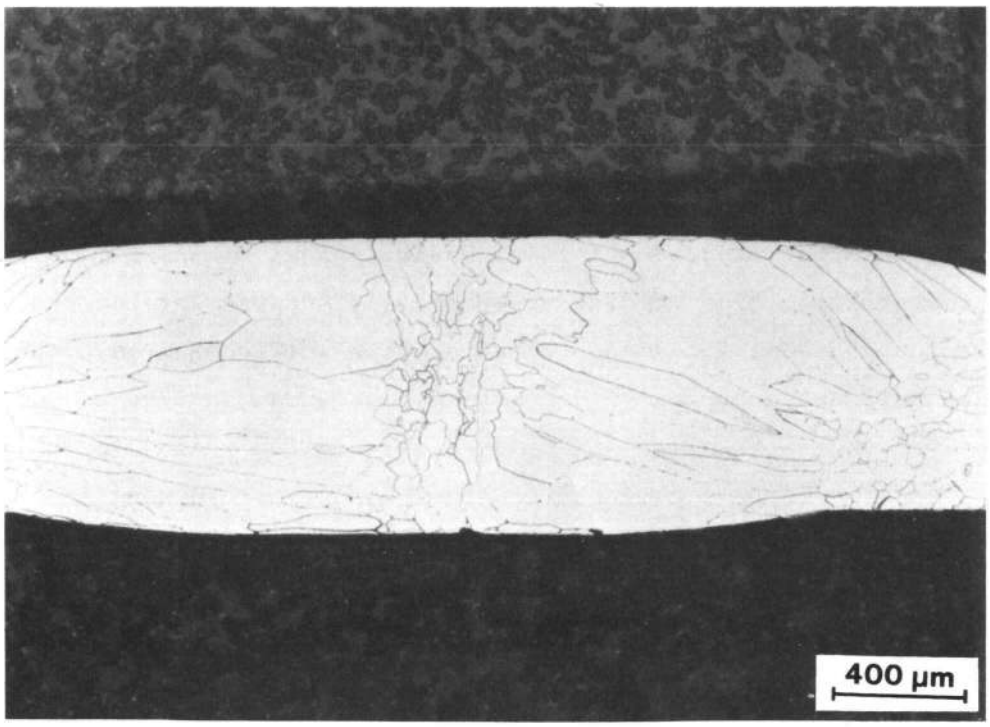

(b)

Fig. 11. Fusion Zone Microstructure of an Arc Weld Without Arc Oscillation. Welding speed: 12.5 mm/s. (a) Top surface. (b) Transverse section.

fusion zone structure along the centerline of the weld shown in Fig. 11 may be attributable to the weld puddle geometry discussed earlier and shown in Fig. 8. The substructure within the grain is not clearly visible because of etching difficulties, and when visible it has been observed to be cellular dendritic.

Figure 12 shows surface and transverse weld microstructures of an arc weld made with 375 cycles/s arc oscillations normal to the welding direction at a welding speed of 12.5 mm/s. Overall fusion zone microstructure appears to be finer than the weld without arc oscillation described above. This refined structure may result from a number of effects brought about by the oscillating motion of the weld puddle. For example, when arc oscillation is employed both the shape of the weld pool and the instantaneous growth rate at the trailing edge of the weld pool can be made to vary with time. Also, the direction and magnitude of the temperature gradients may be altered periodically as the heat source is oscillated, leading to variations in the weld pool solidification conditions.

The investigations also revealed that along the length of the welds the fusion zone microstructure varied slightly from region to region. Also, microstructures of the butt welds examined were similar to the bead-on-plate weld.

Laser Welds

Figure 13 shows the surface and root bead profiles of the laser welds at various welding speeds on a 0.65-mm-thick coupon. The weld surface was smooth and defect free. The surface characteristics are essentially similar to electron beam welds except for a wider bead width. On an average, surface bead width was about 2.0 mm, and the root was 1.5 mm. In the range of welding speeds investigated, the puddle shape appears to be elliptical. The tendency of the puddle to be teardrop shaped increases as the welding speed increases.

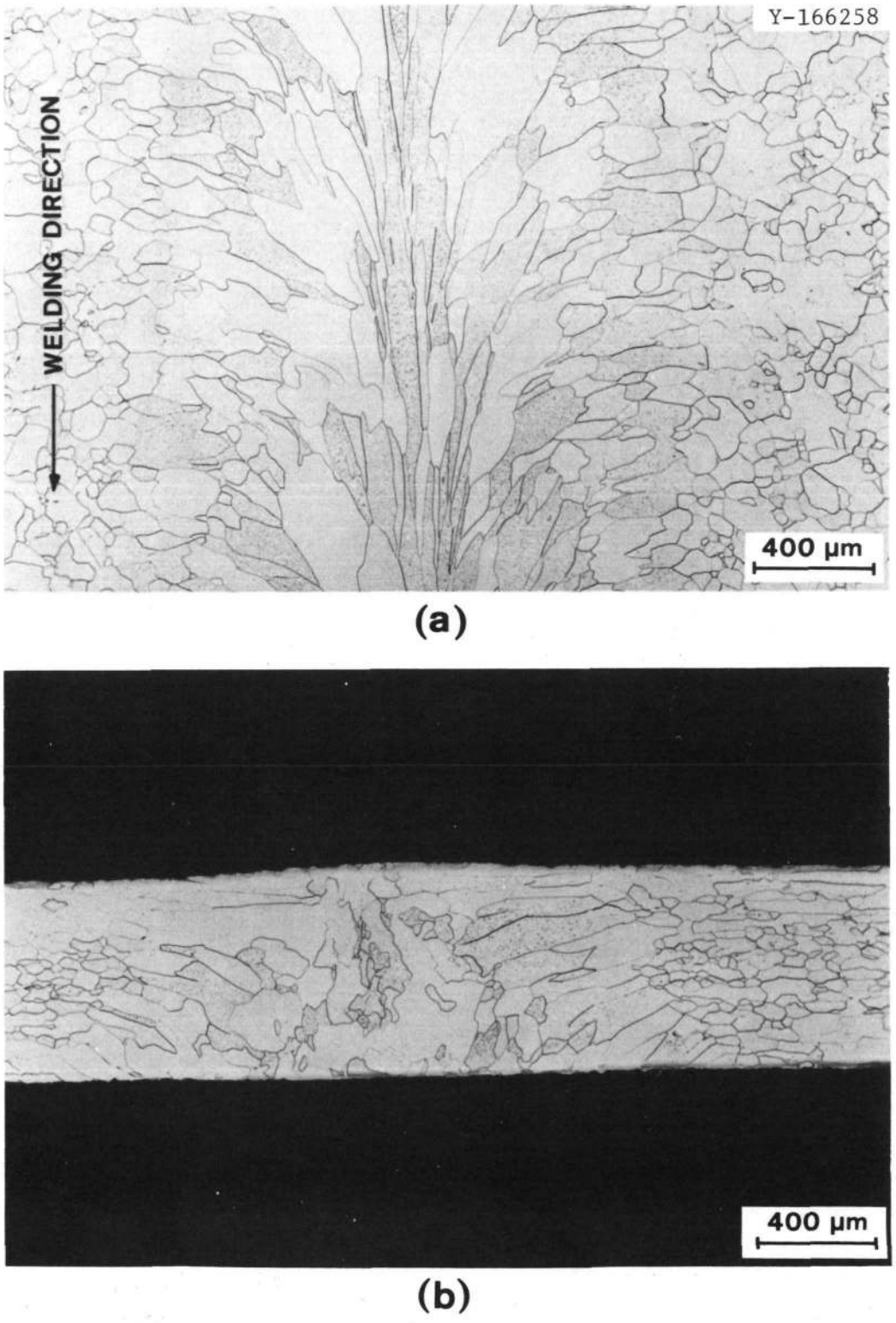

Fig. 12. Fusion Zone Microstructure of an Arc Weld with 375 cycles/s Arc Oscillation. Welding speed: 12.5 mm/s. (a) Top surface. (b) Transverse section.

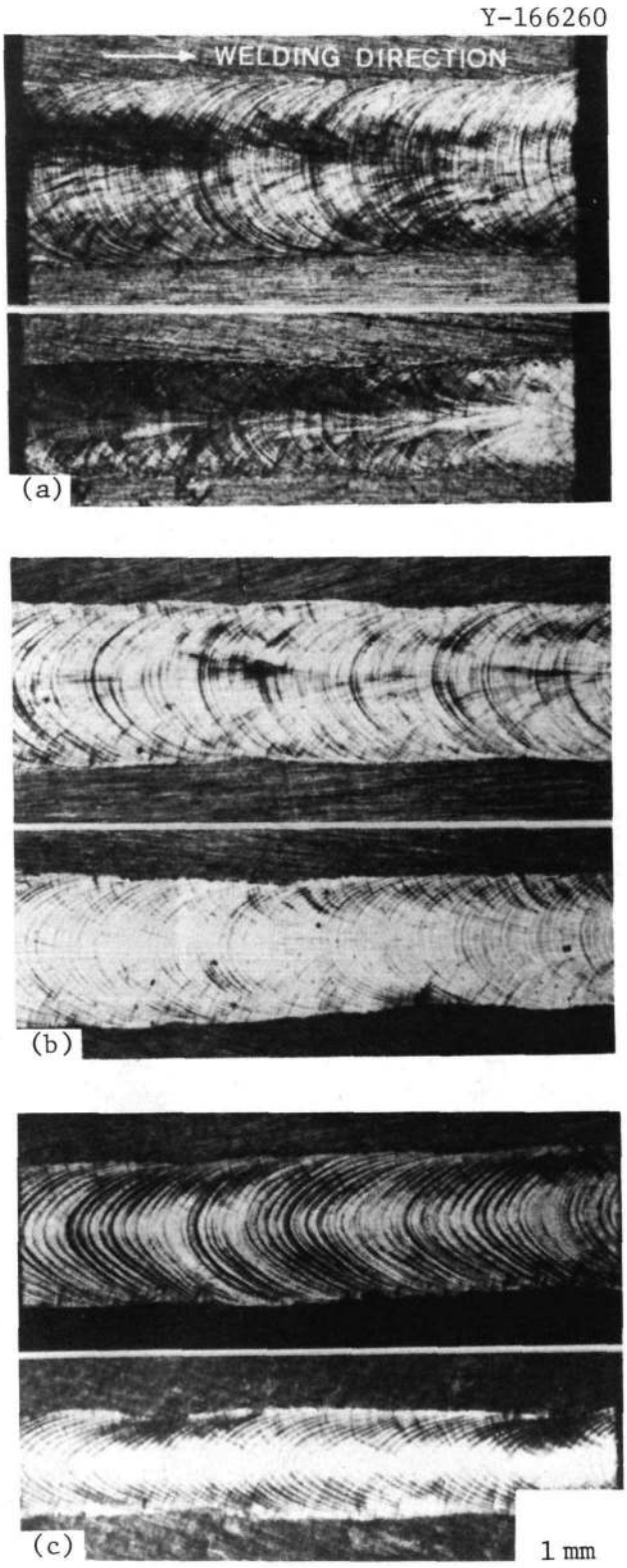

Fig. 13. Surface and Root Laser Weld Bead Profiles at Various Welding Speeds. (a) 8.3 mm/s. (b) 12.5 mm/s. (c) 16.7 mm/s.

Figure 14 shows a typical microstructure of an autogenous bead-on-plate laser weld made at 8.3 mm/s. The weld puddle shape of this weld appears to be elliptical. The fusion zone microstructure [Fig. 14(b)] appears to be significantly refined compared with the arc weld made without arc oscillation and somewhat similar to the arc weld made with arc oscillation shown in Fig. 12. This results from the highly concentrated heat source available in the laser beam and the high thermal gradient, which provide solidification rates one to two orders of magnitude faster than those associated with other conventional fusion welding techniques. Except for a few grains growing along the welding direction, most of the grains exhibit considerable curvature. For an elliptically shaped weld puddle, the direction of maximum thermal gradient changes continually from the fusion boundary to the weld centerline. As a result no one grain experiences favored growth for an extended period. Hence, many grains from the fusion line survive to reach the centerline of the weld. Also the grains that survive to reach the centerline exhibit considerable curvature, as shown in Fig. 14. This was shown earlier in the schematic in Fig. 8(b). As in arc welds, solidification substructure within the grains of the fusion zone is not very clear at low magnification. However, it can be discerned at high magnification, as shown in Fig. 15. The solidification substructure is predominantly cellular dendritic.

Figure 16 shows typical surface and transverse microstructures of laser welds obtained at 16.7 mm/s. The fusion zone microstructure appears to be somewhat finer than that observed in the weld made at 8.3 mm/s (Fig. 14) or in the arc weld shown in Fig. 12. This mainly results from the added influence of higher welding speed in addition to the other factors discussed earlier. The microstructures of the butt welds were examined and compared with bead-on-plate welds and were comparable in structure to them.

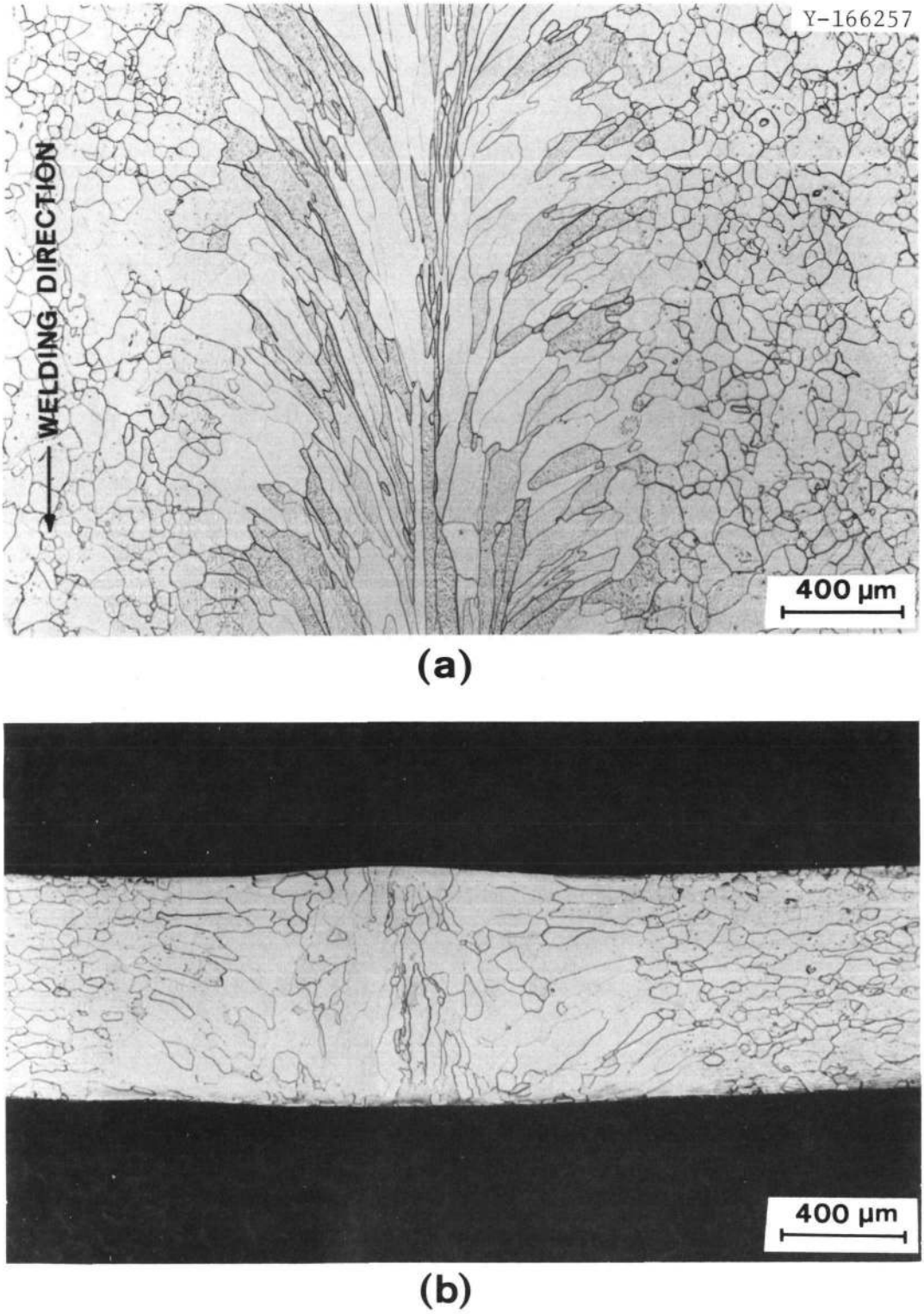

Fig. 14. Fusion Zone Microstructure of a Laser Weld. Welding speed: 8.3 mm/s. (a) Top surface. (b) Transverse section.

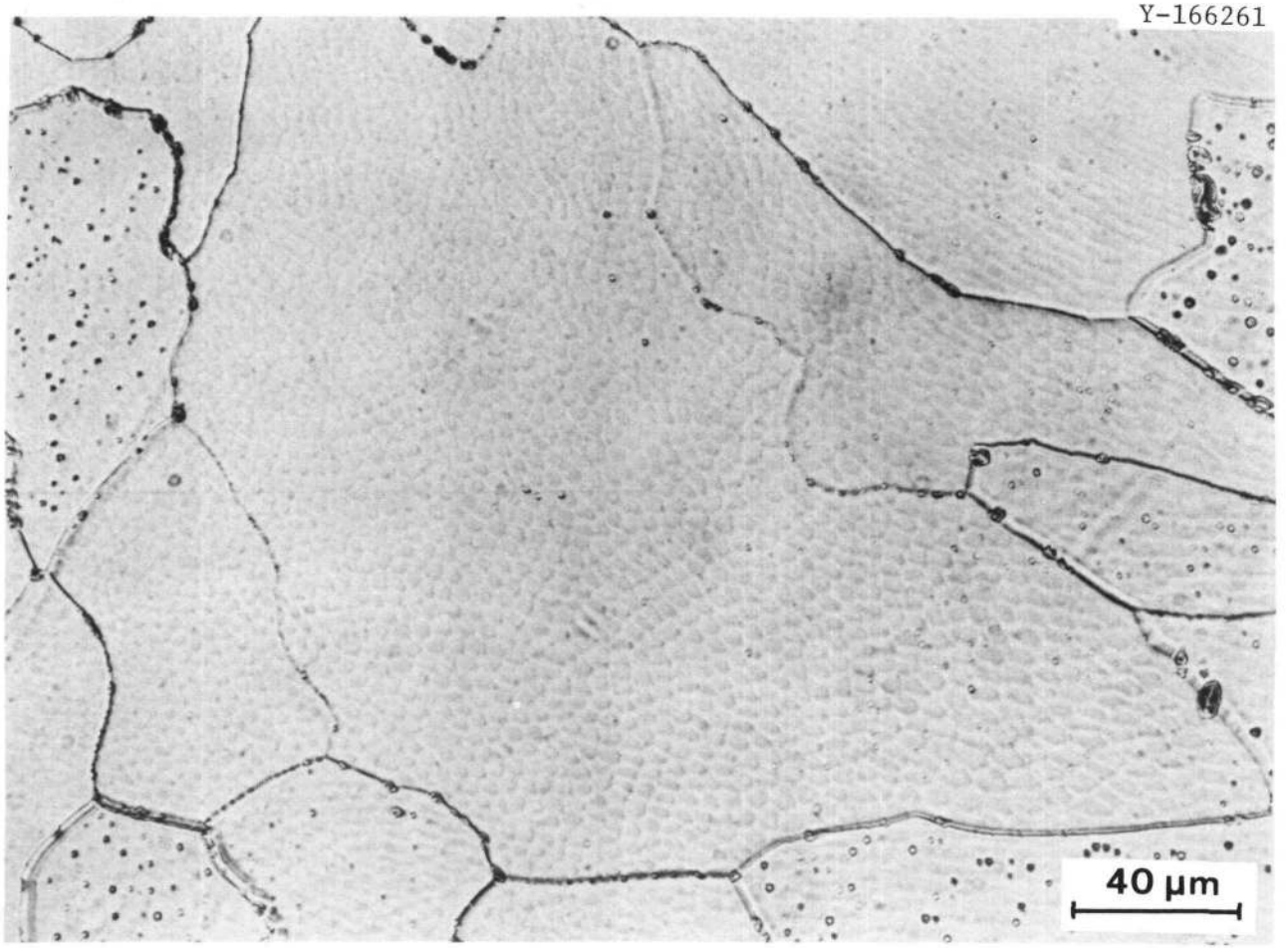

Fig. 15. The Solidification Substructure Within the Grain is Predominantly Cellular Dendritic.

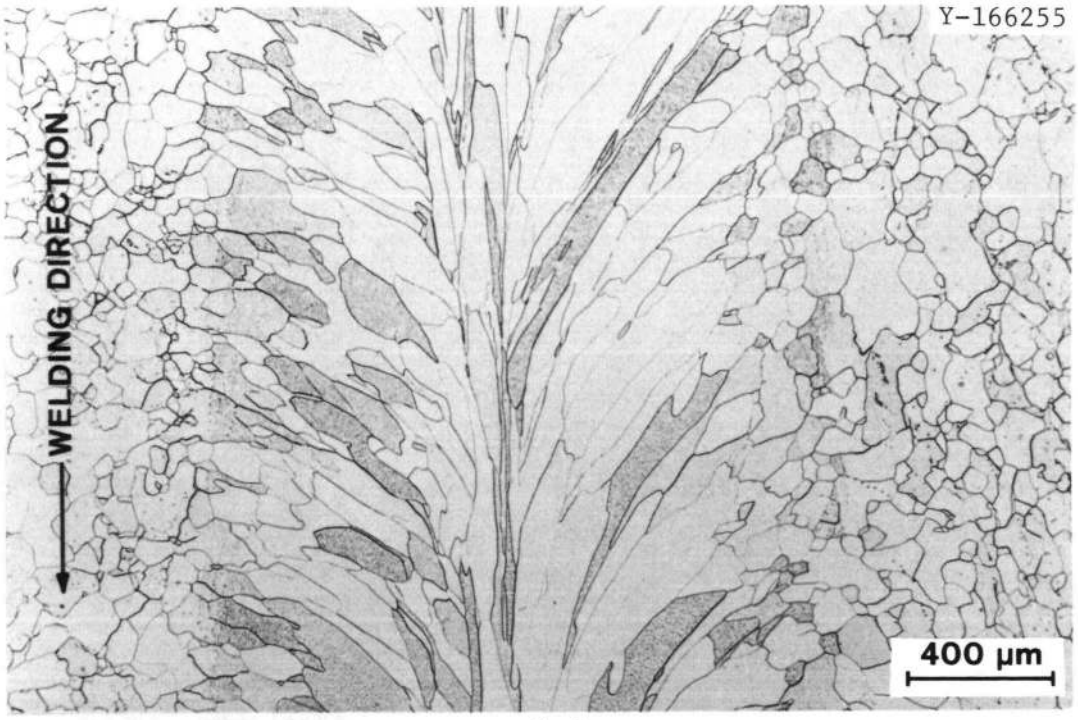

(a)

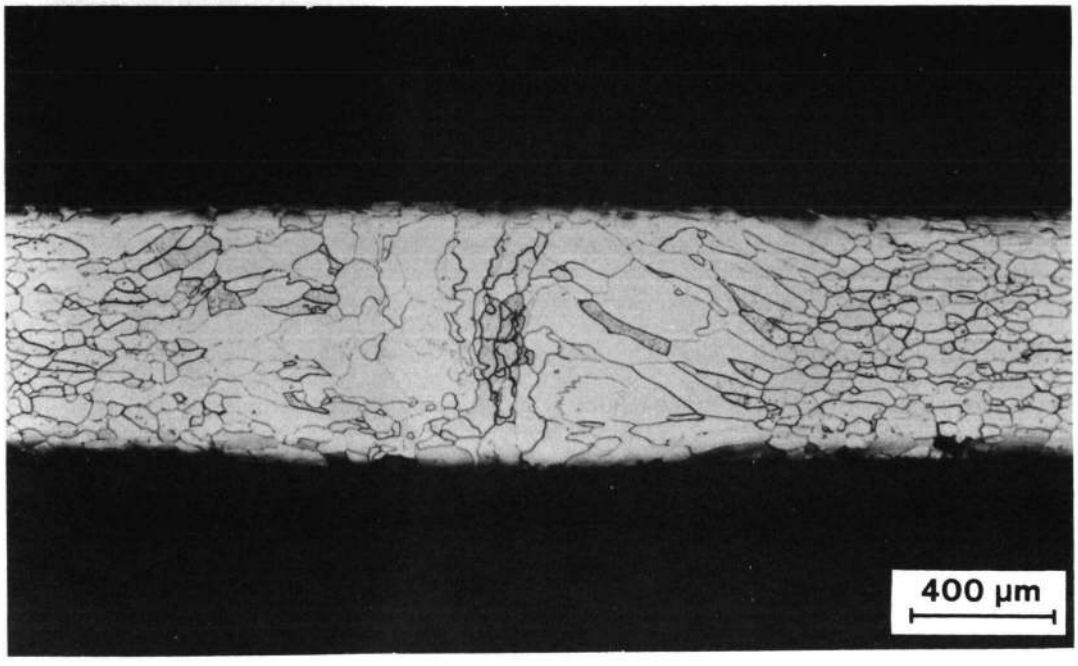

(b)

Fig. 16. Fusion Zone Microstructure of a Laser Weld. Welding speed: 16.7 mm/s. (a) Top surface. (b) Transverse section.

SUMMARY

An extensive weldability study using the GTA process to weld iridium alloy containing 200 wt ppm Th (DOP-14) revealed severe hot cracking during welding. The weld metal cracking resulted from the combined effects of HAZ liquation cracking and solidification cracking. Scanning electron microscopy of the fractured surface revealed patches of low-melting eutectic.

Successful laser welds without hot cracking have been made in DOP-14 alloy. This results from the characteristics of a highly concentrated heat source available in the laser and from the refinement in fusion zone structure. The fusion zone structure is a strong function of the welding speed.

Attempts to refine the fusion zone structure of the iridium alloy (DOP-26) to improve the impact properties by oscillating the welding arc under controlled conditions have been somewhat successful. The fusion zone structure of the arc weld made with arc oscillations during welding appears finer than in the weld made without arc oscillation. This may be attributable to the variations in the shape of the weld pool and to instantaneous growth rate at the edge of the weld pool with time during arc oscillation. No significant variations in fusion zone structure of the autogenous bead-on-plate welds and butt welds were observed.

Laser welds with refined fusion zone structure have been made on DOP-26 alloy. The fusion zone structure of the laser welds compares well with the best structures of the arc welds produced by using arc oscillations.

Finally, the above information on laser welding is only preliminary. An extensive investigation of welding parameters and their influence on the fusion zone structure is needed. Such an investigation could lead to much better fusion zone structure and associated properties than is obtainable presently.

ACKNOWLEDGMENTS

The authors gratefully acknowledge the encouragement of C. O. Tarr of DOE and A. C. Schaffhauser as program manager. Also, the authors wish to acknowledge D. A. Chaplick and L. B. Spiegel of Avco Everett Metalworking Lasers for supplying the necessary information and photographs of an AVCO HPL laser system. Thanks are also due to C. L. White for the scanning electron micrograph and C. P. Haltom for metallography. Finally, we acknowledge H. Inouye and J. F. King for technical reviewing, B. G. Ashdown for editing, and K. A. Witherspoon for preparing the manuscript for publication.

REFERENCES

1. C. T. Liu and H. Inouye, *Development and Characterization of an Improved Ir–0.3 W Alloy for Space Radioisotopic Heat Sources*, ORNL-5290 (October 1977).
2. S. A. David and C. T. Liu, "Weldability and Hot-Cracking in Thorium Doped Iridium Alloys," *Met. Technol.* 7: 102–06 (March 1980).
3. C. T. Liu and S. A. David, Oak Ridge National Laboratory, unpublished data.
4. D. L. Coffey, W. H. Jones, W. B. Artnmill, and W. A. Saul, "Parametric Modification of Weld Microstructure in Iridium," *Weld. J.* 53(12): 566-s–568-s (1974).
5. S. A. David, Oak Ridge National Laboratory, unpublished data.
6. P. P. Puzak, W. R. Apblett, and W. S. Pellini, "Hot Cracking of Stainless Steel Weldments," *Weld. J.* 53(1): 96-s–175-s (1956).
7. W. R. Apblett and W. S. Pellini, "Factors Which Influence Weld Hot Cracking," *Weld. J.* 33(2): 83-s–90-s (1954).
8. J. C. Borland, "Hot Cracking in Welds," *Br. Weld. J.* 7: 558–59 (1960).
9. F. C. Hull, "Effects of Delta Ferrite on the Hot Cracking of Stainless Steel," *Weld. J.* 46(8): 399-s–409-s (1967).

10. J. Vero, *Met. Ind. (London)* 48: 431–37 (1936).

11. A.R.E. Singer and P. H. Jennings, "Properties of the Al-Si 1035 Alloys at Temperatures in the Region of the Solidus," *J. Inst. Met.* 73: 33–54 (1946).

12. A.R.E. Singer and P. H. Jennings, "Hot-Shortness of Some High Purity Alloys," *J. Inst. Met.* 74: 227–40 (1947).

13. W. S. Pellini, "Strain Theory of Hot Tearing," *Foundry* 80: 124–33 (1952).

14. J. C. Borland, "Generalized Theory of Super Solidus Cracking in Welds and Castings," *Br. Weld. J.* 7: 508–512 (1960).

15. C. S. Smith, "Grains, Phases and Interfaces," *Trans. AIME* 175: 15–51 (1948).

16. A. L. Schawlow and C. H. Townes, "Infrared and Optical Masers," *Phys. Rev.* 112(6): 1940–49 (December 1958).

17. T. H. Maiman, "Stimulated Optical Radiation in Ruby," *Nature* 187: 493–94 (August 1960).

18. S. S. Charschan, Ed., *Lasers in Industry*, Van Nostrand Reinhold Co., New York, 1972.

19. J. F. Ready, *Effects of High-Power Laser Radiation*, Academic Press, New York, 1971.

20. J. E. Gevsic, H. M. Marcos, and L. G. VanVitert, "Laser Oscillations in Nd-Doped Yttrium Aluminum, Yttrium Gallium and Gadolinium Garnets," *Appl. Phys. Lett.* 4(10): 182–84 (May 1964).

21. C.K.N. Patel, "Continuous-Wave Laser Action on Vibrational-Rotational Transitions of CO_2," *Phys. Rev.* 136(5A): A1187–A1193 (November 1964).

22. C. O. Brown, "High Power CO_2 Electric Discharge Mixing Laser," *Appl. Phys. Lett.* 17(19): 388–91 (1970).

23. J. W. Davis and C. O. Brown, "Electric Discharge Convective Lasers," paper presented at the AIAA 5th Flux and Plasma Dynamics Conference, Boston, June 1972.

24. W. C. Ball and C. M. Banas, *Metal Working Capability of a High Power Laser, SAE Rep.* 740864 (1974).

25. E. Locke, E. Hoag, and R. Hella, "Deep Penetration Welding with High Power CO_2 Lasers," *Weld. J.* 51(5): 245-s–249-s (May 1972).

26. E. L. Baardsen, D. J. Schmata, and R. E. Bisaro, "High Speed Welding of Sheet Steel with a CO_2 Laser," *Weld. J.* 52(4): 227–29 (April 1973).

27. C. L. White, "The Effect of Trace Element Additions on the Grain Boundary Composition of Ir + 0.3% W Alloys," *Metall. Trans.* 10A: 683–92 (1979).

28. J. R. Thomson, "Alloys of Thorium with Certain Transition Metals II, The Systems Thorium-Osmium, Thorium-Iridium, and Thorium-Platinum," *J. Less-Common Met.* 6: 3–4 (1964).

29. H. Kleykamp, "Thermodynamische Untersuchvngend in der Systemen Thorium-Osmium and Thorium-Iridium," *J. Less-Common Met.* 63: 25–33 (1979).

page blank

INTERNAL DISTRIBUTION

1–2. Central Research Library
3. Document Reference Section
4–5. Laboratory Records Department
6. Laboratory Records, ORNL RC
7. ORNL Patent Section
8. D. N. Braski
9–13. S. A. David
14. R. G. Donnelly
15. J. A. Carter
16. L. D. Frye
17. G. M. Goodwin
18. D. E. Harasyn
19. R. L. Heestand
20–22. M. R. Hill
23. H. Inouye
24. J. F. King
25. J. S. Lin
26–30. C. T. Liu
31. J. W. McEnerney
32. A. J. Moorhead
33–37. A. C. Schaffhauser
38. G. M. Slaughter
39. C. L. White
40. A. L. Bement, Jr. (Consultant)
41. W. R. Hibbard, Jr. (Consultant)
42. E. H. Kottcamp, Jr. (Consultant)
43. Alan Lawley (Consultant) ultant)
44. M. J. Mayfield (Consultant)
45. J. T. Stringer (Consultant)

EXTERNAL DISTRIBUTION

46. Air Force Weapons Laboratory, Kirtland Air Force Base, DYUS, Albuquerque, NM 87116

    Michael Seaton

47–48. Battelle Columbus Laboratories, 505 King Ave., Columbus, OH 43201

    E. L. Foster
    I. M. Grinberg

49–50. E. I. du Pont de Nemours, Savannah River Plant, Aiken, SC 29801

    R. A. Brownback
    W. R. Kanne

51–52. E. I. du Pont de Nemours, Savannah River Laboratory, Aiken, SC 29801

    R. T. Huntoon
    R. H. Tait

53–54. Fairchild Industries, 20301, Century Blvd., Germantown, MD 20767

    M. Eck
    A. Schock

55. General Atomic Co., P.O. Box 81608, San Diego, CA 92138

    N. B. Elsner

56–58. General Electric Co., Vally Forge Space Center, P.O. Box 8048, Philadelphia, PA 19101

V. Haley
R. J. Hemler
C. W. Whitmore

59–61. Jet Propulsion Laboratory, California Institute of Technology, 4800 Oak Grove Drive, Pasadena, CA 91103

R. W. Campbell
J. E. Mondt
A. E. Wolfe

62. Johns Hopkins University, Applied Physics Laboratory, Johns Hopkins Road, Laurel, MD 20810

J. C. Hagan

63–65. Los Alamos Scientific Laboratory, P.O. Box 1663, Los Alamos, NM 87545

R. D. Baker
S. E. Bronisz
S. S. Hecker

66–69. Minnesota Minining and Manufacturing Co., St. Paul, MN 55101

R. B. Ericson
E. F. Hampl
J. D. Hinderman
W. C. Mitchell

70–71. Monsanto Research Corp., P.O. Box 32, Miamisburg, OH 45342

E. W. Johnson
W. C. Wyder

72. Sundstrand Energy Systems, 4747 Harrison Ave., Rockford, IL 61101

E. Krueger

73–74. Teledyne Energy Systems, 110 W. Timonium Rd., Timonium, MD 21093

W. J. Barnett
W. E. Osmeyer

75–87. DOE Division of Advanced Nuclear Systems and Projects, Washington, DC 20545

G. L. Bennett
R. C. Brouns
F. M. Dieringer
N. Goldenberg
J. S. Griffo
W. D. Kenney
J. J. Lombardo
R. B. Morrow
P. A. O'Riordan
W. C. Remini
B. J. Rock
C. O. Tarr
N. R. Thielke

88–89. DOE Albuquerque Operations Office, P.O. Box 5400, Albuquerque, NM 87115

D. K. Nowlin
D. Plymale

90. DOE Dayton Area Office, P.O. Box 66, Miamisburg, OH 45342

H. N. Hill

91–92. DOE Oak Ridge Operations Office, P.O. Box E, Oak Ridge, TN 37830

J. A. Lenhard
J. Pidkowicz

93–94. DOE San Francisco Operations Office, 1333 Broadway, Wells Fargo Building, Oakland, CA 94612

L. Lanni
W. L. Von Flue

95–96. DOE Savannah River Operations Office, P.O. Box A, Aiken, SC 29801

W. T. Goldston
W. D. Sandberg

97–123. DOE, Technical Information Center, Office of Information Services, P.O. Box 62, Oak Ridge, TN 37830

☆U.S. GOVERNMENT PRINTING OFFICE: 1980-640-245/067